



Chiral-induced spin selectivity: A polaron transport model

Longlong Zhang* and Yuying Hao

College of Physics and Optoelectronics, Taiyuan University of Technology, Taiyuan 030024, China

Wei Qin and Shijie Xie†

*School of Physics, State Key Laboratory of Crystal Materials, Shandong University, Jinan 250100, China*Fanyao Qu *Institute of Physics, International Center for Condensed Matter Physics, University of Brasilia, Brasilia 70919-970, Brazil* (Received 16 September 2020; revised 19 November 2020; accepted 30 November 2020; published 14 December 2020)

Weak hyperfine interactions and spin-orbit coupling (SOC) in organic materials result in long spin lifetimes, which is very promising for spintronics. On the other hand, they also make it challenging to achieve spin polarization, which is of crucial importance for spintronics devices. To overcome this obstacle, we have proposed a physical model for spin-polarized electron transport through a chiral molecule based on the chiral-induced spin selectivity. Because the transport in the chiral molecule is not an isolated one, but rather an electron coupled to its surrounding lattice distortions, namely, a spatial localized polaron, an indispensable polaron effect is incorporated in our model. We show that the polaron transport through the chiral molecule exhibits a spin-momentum-locked feature. Interestingly, no matter what their initial spin state is, all of the polarons could transmit through the molecule with their spins being aligned to the same orientation due to the effective “inverse Faraday effect.” The coexistence of the electron-lattice coupling and SOC results in the spin and lattice being coupled, which leads to a strongly enhanced spin coherence and then a very high spin polarization of 70%. In addition, the effects of the helix pitch, polaron size, and drift velocity on spin polarization are also discussed. Our results open the possibility of using chiral molecules in spintronics applications and offer a paradigm for information processing and transmission.

DOI: [10.1103/PhysRevB.102.214303](https://doi.org/10.1103/PhysRevB.102.214303)**I. INTRODUCTION**

A chiral molecule is one that lacks inversion symmetry and is not superimposable on its mirror image. Fascinatingly, chiral molecules can act as efficient sources of spin-polarized electrons even in the absence of heavy nuclei, magnetic doping, or the application of external magnetic field due to chiral-induced spin selectivity (CISS) effect; that is, the electron transmission through the molecule is preferential for one spin orientation over the other one [1–6]. Since many biomolecules are chiral, the discovery of CISS opens a window for exploring biomolecule-based spintronic devices with no magnets. To date, the CISS effect has been experimentally observed in several organic systems such as DNA [7,8], bacteriorhodopsin [9], oligopeptides [10], etc. Meanwhile, to explain the experimental data, a few theoretical models as well as density function theory calculations have been proposed [11–17]. By assuming an unrealistically large spin-orbit coupling (SOC), measurable spin polarization (SP) could be realized. To make up for this theoretical deficit, Gutierrez *et al.* presented a minimal tight-binding model to investigate the transport of an electron through a helically shaped electric field (HEF). They concluded that to achieve

the high SP in weak SOC materials, the chiral molecule should exhibit a less dispersive electronic band and low charge mobility [18].

We notice that, in all calculations reported in the literature, the chiral molecule was supposed to be rigid and the Landauer-Buttiker theory was employed [15,18,19]. As is already known, in organic chiral molecules, there are strong electron-lattice (*e-l*) couplings, giving rise to the formation of a polaron (see the white curves in Fig. 1 labeled P). It is a kind of spatially localized charged quasiparticle with spin $\pm \frac{\hbar}{2}$. In addition, the polaron has a relatively large effective mass and low mobility (lower than the acoustic velocity). Thus, it meets perfectly the low-mobility requirement for achieving high SP. Therefore, the most important carrier in organic materials is the polaron, instead of the free electron. However, the role played by polarons in CISS was never investigated in previous theories.

In this work, we study spin polaron transport through a chiral molecule with spin-related quantum dynamics. The results show that, driven by a static electric field E_z , both spin-up (P_\uparrow) and spin-down (P_\downarrow) polarons can pass through the chiral molecule, but with different spin dynamics: the spin parallel to the drift velocity will keep its orientation, while the antiparallel one will undergo spin switchings (see Fig. 1). Our results are in contrast to those previously proposed such as the free-charge scattering mechanism, where only one spin

*longlongzhang@tyut.edu.cn

†xsj@sdu.edu.cn

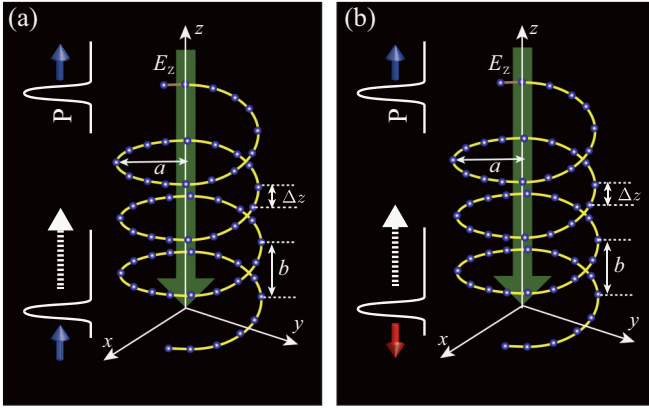


FIG. 1. Schematic illustrations of (a) the spin-up (see blue arrow in the lower part) and (b) spin-down (see red arrow in the lower part) polaron (white curves labeled by P) propagation through a chiral molecule driven by a static z -direction electric field E_z (green arrows indicate the E_z direction, and white dotted arrows indicate the polaron drift direction). In both cases, the final stabilized spin state is orientated up (see blue arrows in the upper part), indicating a clear spin-momentum-locked character. The notations b , a , and Δz denote the helix pitch, helix radius, and z -direction distance between two neighboring sites, respectively. Referring to the example of B-DNA, the parameters can be set as $b \sim 3.2$ nm, $a \sim 0.7$ nm, and $\Delta z \sim 0.32$ nm [18].

component is allowed to pass through the helically shaped potential. Then the high SP is compensated by the reduction of current intensity. Here, because all of the charge carriers' spins are totally aligned to the same orientation, SP can be as high as 70%.

II. MODEL AND FORMULATION

We depict the chiral molecule using the Hamiltonian

$$\mathcal{H} = \mathcal{H}_e + \mathcal{H}_h. \quad (1)$$

\mathcal{H}_e is the extended Peierls-Hubbard Hamiltonian, which was used to describe the conventional molecule without chirality [20,21]:

$$\begin{aligned} \mathcal{H}_e = & - \sum_{j,s} t_j (c_{j,s}^\dagger c_{j+1,s} + \text{H.c.}) \\ & + \frac{K}{2} \sum_j (u_{j+1}^2 - u_j^2) + \frac{M}{2} \sum_j \dot{u}_j^2 \\ & + U \sum_j \left(n_{j,\uparrow} - \frac{1}{2} \right) \left(n_{j,\downarrow} - \frac{1}{2} \right) \\ & + V \sum_j \sum_{s,s'} (n_{j,s} - 1)(n_{j+1,s'} - 1). \end{aligned} \quad (2)$$

Here, $t_j = t_0 + (-1)^j t_e - \alpha [u_{j+1}(t) - u_j(t)]$ is the hopping integral between sites j and $j+1$, with t_0 being the nearest-neighbor transfer integral for a uniform lattice structure and t_e being the symmetry-breaking parameter introduced to lift the ground-state degeneracy in nondegenerate polymers; u_j denotes the z direction displacement of the j th site from its equilibrium position, and α is the e - l coupling constant. The

second line of Eq. (2) describes the elastic and kinetic energies of lattices, where K denotes the elastic constant and M is the single site's mass. U represents the on-site Coulomb interactions, and V is the strength of the nearest-neighbor Coulomb interactions; the notation $n_{j,s}$ denotes the spin- s electron density operator on site j .

\mathcal{H}_h in Eq. (1) is the Hamiltonian related to the chirality symmetry of the molecule, acting as a HEF on the particle. The analytical results for such a HEF were derived in Ref. [18] and are expressed as

$$\mathbf{E}_h = -E_0 \sum_{l,i} g_{l,i}(z) [\cos(Qi\Delta z), \sin(Qi\Delta z)], \quad (3)$$

where $g_{l,i}(z) = \{1 + [(z - lb - i\Delta z)/a]^2\}^{-3/2}$ and $Q = 2\pi/b$. The configurations of the chiral molecule are labeled by a , b , and Δz (see Fig. 1). Index l counts the helix turn number, and i labels the atomic site along one turn of the helix. Assuming one helix turn contains N_0 sites, $N_0\Delta z \equiv b$. The constant E_0 is determined by the charge density at each site and the helix radius. One charge passing through this HEF along the z axis leads to an effective SOC: $H_{\text{SOC}} = \lambda \boldsymbol{\sigma}(\mathbf{p} \times \mathbf{E}_h)$, with $\lambda = \hbar/2mc$ being the SOC strength, \mathbf{p} being the polaron momentum, and $\boldsymbol{\sigma}$ being a vector whose components are the Pauli matrices σ_x , σ_y , and σ_z . As the polaron propagates along the z direction, we will assume $p_x = p_y = 0$, $p_z \neq 0$. We assume the periodic boundary condition of the molecule and $\mathbf{E}_h(z) = \mathbf{E}_h(z + mb)$, $m = 1, 2, \dots$. Under such circumstances, the distribution of $\mathbf{E}_h(z)$ becomes dependent on only the change in the helix angle, namely, $\mathbf{E}_h(z) = -E_0 G_0 \exp(-iQj\Delta z)$, where the index $j \equiv (l-1)N_0 + i$ runs along all the sites and G_0 is a constant whose value is related to the helix geometry parameters. Applying a standard second quantization procedure, the helix-symmetry effect is finally described as the following effective tight-binding model [22]:

$$\begin{aligned} \mathcal{H}_h = & t_{\text{S-O}} \sum_j (e^{-ij\omega} c_{j,\uparrow}^\dagger c_{j,\downarrow} + e^{ij\omega} c_{j,\downarrow}^\dagger c_{j,\uparrow}) \\ & + t_{\text{S-I}} \sum_j (e^{-ij\omega} c_{j+1,\uparrow}^\dagger c_{j,\downarrow} - e^{-ij\omega} c_{j,\uparrow}^\dagger c_{j+1,\downarrow} \\ & - e^{ij\omega} c_{j+1,\downarrow}^\dagger c_{j,\uparrow} + \exp^{ij\omega} c_{j,\downarrow}^\dagger c_{j+1,\uparrow}), \end{aligned} \quad (4)$$

where $t_{\text{S-O}} = -i\omega\beta/\Delta z$ and $t_{\text{S-I}} = \beta/2\Delta z$ denote the on-site and intersite SOC strengths, respectively ($\beta = \lambda\hbar G_0 E_0$), and $\omega = 2\pi/N_0$ denotes the change in the helix angle when the electron propagates a distance Δz . Notice that the SOC here originates from the helix structure rather than from the atoms. It is worthwhile to recall that to preserve the Hamiltonian \mathcal{H}_h as Hermitian, a symmetrization procedure, in which the small phase factor determined by ω is neglected, is carried out [22]. Since Eq. (4) possesses time-reversal symmetry, one cannot expect SOC alone to generate any SP.

In the following, unless otherwise noted, we set the parameters [23–26] $t_0 = 30$ meV, $t_1 = 0.2 t_0$, $U = 0.8 t_0$, $V = 0.2 t_0$, $K = 630$ meV/Å², $\alpha = 120$ meV/Å, $M = 26$ meV ps²/Å², $t_{\text{S-I}} = 0.08 t_0 = 2.4$ meV, $N_0 = 40$. At half filling, the self-consistent calculation of Eq. (1) gives rise to the Peierls-gapped ground state with the lattices being dimerized. Further injecting one electron at the lowest unoccupied

molecular orbital of the gapped ground state leads to the formation of a negatively charged polaron. The polaron-induced lattice distortions can be identified by the smoothed bond orders, defined as $\tilde{y}_j(t) = (-1)^j[2y_j(t) - y_{j-1}(t) - y_{j+1}(t)]$, with $y_j(t) = u_{j+1}(t) - u_j(t)$ being the change in bond length between sites j and $j + 1$. Meanwhile, the polaron possesses either a spin-up or spin-down state of 50%. It is evaluated by the spin-density distributions $s_j^z(t) = \langle n_{j,\uparrow}(t) \rangle - \langle n_{j,\downarrow}(t) \rangle$. The static lattice configuration and the spin distributions of a static polaron are demonstrated in Fig. 2(a) [black curve for \tilde{y}_j and red (blue) curve for spin-down (spin-up) distributions]. It can be recognized that the polaron size is around $20\Delta z$ along the z axis.

Electric field E_z drives the polaron to propagate along the molecule chain. The effect induced by E_z can be simulated by adding a phase factor $e^{-i\gamma A(t)}$ ahead of the hopping term [27,28]:

$$c_{j,s}^\dagger c_{j+1,s} \rightarrow e^{-i\gamma A(t)} c_{j,s}^\dagger c_{j+1,s}, \quad (5)$$

where the coefficient γ is taken as $\gamma = e\Delta z/\hbar c$, with e being the electron charge and c being the velocity of light; the time-dependent vector potential A_t reads

$$A(t) = -cE_z t. \quad (6)$$

Then, the Hamiltonian of the chiral molecule subjected to an electric field E_z becomes

$$\begin{aligned} \mathcal{H}(t) = & - \sum_{j,s} t_j [e^{-i\gamma A(t)} c_{j,s}^\dagger c_{j+1,s} + \text{H.c.}] \\ & + \frac{K}{2} \sum_j (u_{j+1}^2 - u_j^2) + \frac{M}{2} \sum_j \dot{u}_j^2 \\ & + U \sum_j \left(n_{j,\uparrow} - \frac{1}{2} \right) \left(n_{j,\downarrow} - \frac{1}{2} \right) \\ & + V \sum_j \sum_{s,s'} (n_{j,s} - 1)(n_{j+1,s'} - 1) \\ & + t_{\text{S-O}} \sum_j (e^{-ij\omega} c_{j,\uparrow}^\dagger c_{j,\downarrow} + e^{ij\omega} c_{j,\downarrow}^\dagger c_{j,\uparrow}) \\ & + t_{\text{S-I}} \sum_j (e^{-ij\omega} c_{j+1,\uparrow}^\dagger c_{j,\downarrow} - e^{-ij\omega} c_{j,\uparrow}^\dagger c_{j+1,\downarrow} \\ & - e^{ij\omega} c_{j+1,\downarrow}^\dagger c_{j,\uparrow} + \exp^{ij\omega} c_{j,\downarrow}^\dagger c_{j+1,\uparrow}). \end{aligned} \quad (7)$$

Notice that $\mathcal{H}(t)$ in Eq. (7) is no longer time-reversal symmetry preserved due to the existence of the phase factor $e^{-i\gamma A(t)}$ ahead of the hopping terms.

The evolution of wave functions of the polaron propagating along the chiral molecule chain is obtained by solving the time-dependent Schrödinger equation:

$$i\hbar \dot{\Psi}^\kappa(t) = \mathcal{H}(t)\Psi^\kappa(t). \quad (8)$$

$\Psi^\kappa(t)$ is the column vector of the κ th orbital wave function, which is expanded as

$$\Psi^\kappa(t) = [\dots \psi_{j,\uparrow}^\kappa(t) \psi_{j+1,\uparrow}^\kappa(t) \dots \psi_{j,\downarrow}^\kappa(t) \psi_{j+1,\downarrow}^\kappa(t) \dots] \quad (9)$$

in Wannier space. A finite \mathcal{H}_h induces the mixing between the spin-up and spin-down components of $\Psi^\kappa(t)$. Simultaneously,

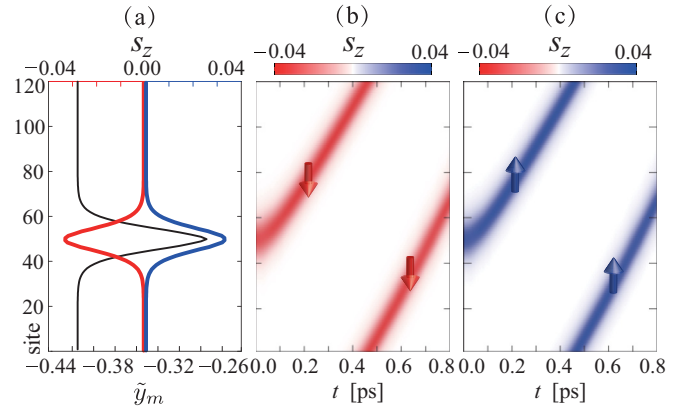


FIG. 2. (a) The lattice-distortion configuration \tilde{y}_j (black) and the spin-density distribution of the polaron with spin $\pm\frac{\hbar}{2}$ (blue and red) at $t = 0$ and time evolutions of $s_{z,j}$ when the polaron is initially (b) spin down and (c) spin up at $eE_z\Delta z = -0.001t_0$ in a chiral molecule but zero HEF is assumed. The periodic boundary condition is adopted to calculate the polaron transport dynamics.

the lattice dynamics are calculated by Newton's equation of motion:

$$\begin{aligned} M\ddot{u}_j(t) = & \alpha[\rho_j(t) - \rho_{j-1}(t)] \\ & + K[u_{j-1}(t) + u_{j+1}(t) - 2u_j(t)], \end{aligned} \quad (10)$$

where $\rho_j = \sum_s \sum_{\kappa} [e^{-\gamma A(t)} \psi_{j,s}^{\kappa*}(t) \psi_{j+1,s}^{\kappa}(t) + \text{H.c.}]$, with \sum_{κ} indicating taking a summation over the occupied orbitals.

III. RESULTS AND DISCUSSION

To gain insight into the mechanism of spin selectivity, let us start with investigating the polaron transport in a chiral molecule by switching off the HEF, namely, $\mathcal{H}_h = 0$, corresponding to conventional molecules. The resultant spin-related dynamics is demonstrated in Figs. 2(b) and 2(c). Obviously, the dynamics of spin-up and spin-down polarons are degenerate. Unless the field strength reaches a threshold at which the polaron is delocalized, the coherence between the local lattice distortion and the spin packet can be kept during the polaron transmissions. We define the SP as $\text{SP} = (I_{\uparrow} - I_{\downarrow})/(I_{\uparrow} + I_{\downarrow})$, where $I_s \equiv D_s \cdot v_s$ is the spin-polarized current, with $D_s \equiv \sum_j s_j^z$ and v_s denoting the spin- s polaron's population and drift velocity, respectively. Since the velocity difference between the two spin-polarized polarons is small, we can take the approximation $\text{SP} = (D_{\uparrow} - D_{\downarrow})/(D_{\uparrow} + D_{\downarrow})$. The calculated SP is zero in Fig. 2.

We proceed to investigate the polaron transport dynamics by switching on the chirality-symmetry effect; namely, the whole Hamiltonian presented in Eq. (1) is used in our calculations. Figure 3 demonstrates the spin-state evolutions of P_{\downarrow} and P_{\uparrow} in a chiral molecule for different z -axis electric fields: $eE_z\Delta z = 0$ [Figs. 3(a1) and 3(a2)], $-0.001t_0$ [Figs. 3(b1) and 3(b2)], and $0.001t_0$ [Figs. 3(c1) and 3(c2)]. For $eE_z\Delta z = 0$, both P_{\downarrow} and P_{\uparrow} remain stationary, i.e., $v_{\uparrow(\downarrow)} = 0$. The spin orientation keeps the initial state without flipping, and therefore, $\text{SP} = 0$. For $eE_z\Delta z = -0.001t_0$, the polaron starts to move toward the $+z$ direction; interestingly, the spin-state evolution differs for P_{\uparrow} and P_{\downarrow} : the former passes

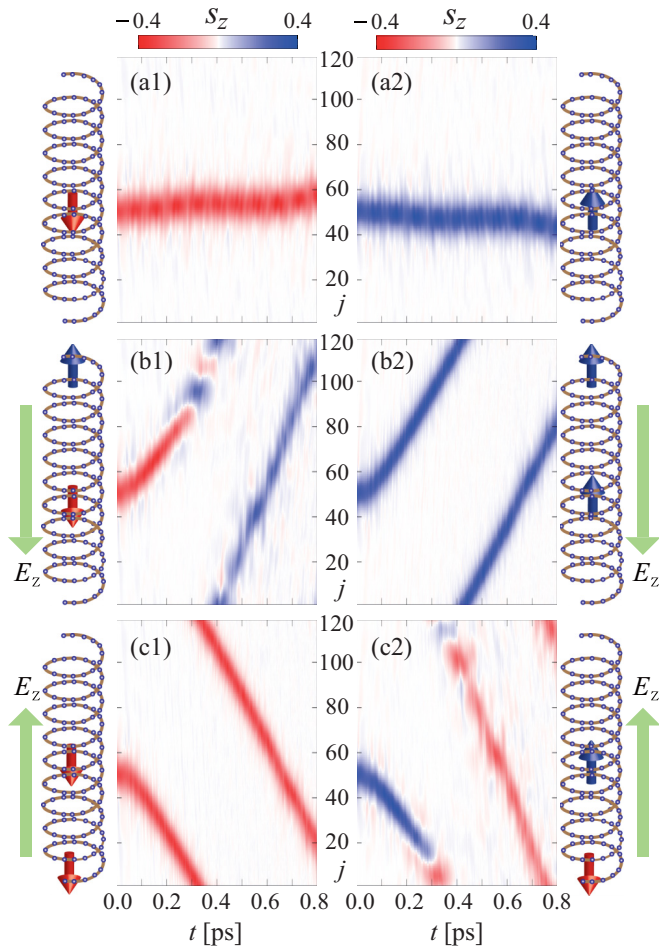


FIG. 3. Time evolutions of s_z^j at (a1) and (a2) $eE_z\Delta z = 0$, (b1) and (b2) $-0.001t_0$, and (c1) and (c2) $0.001t_0$ for the polaron with initial spin-down (left column) and spin-up (right column) states in chiral molecules.

through the helix molecule without feeling the existence of the HEF, while the latter undergoes spin switching after passing a certain distance. Consequently, all the polaron spins are finally aligned to the same orientation. Therefore, the SP reaches as high as 70%. In addition, unlike the scattering model [29,30] and the spin-associated charge tunneling model [31], there is no charge loss during the transmission. For $eE_z\Delta z = 0.001t_0$, the polaron moves along the opposite direction and feels the opposite-helicity HEF. Therefore, it changes to be that P_\downarrow is not affected by the HEF and P_\uparrow undergoes spin switching. It can be concluded that the spin dynamics is coupled to the polaron momentum in a chiral molecule.

It is heuristic to compare the physics revealed in Fig. 3 with the spin-associated dynamics in two other common cases, e.g., conventional organic molecules and rigid chiral molecules. In conventional organic molecules, SOC is absent, while in rigid chiral molecules, e - l coupling is missing. In the former, the SP is zero (Fig. 2). In the latter, although SP is nonzero, it is usually quite small. Differently, both SOC and e - l coupling are involved in our model. This builds a bridge between the degrees of freedom of the spin and lattice. Remember that, for conventional spin transport in inorganic semiconductors,

usually, the SP is small because of the short coherence time caused by various scattering channels. When spins and lattices are strongly coupled as in spin polarons, however, the spin coherence is significantly enhanced due to reduced scattering channels because of their larger mass. Hence, the SP can be very high.

We propose the mechanism of the helicity-dependent spin switching presented in Figs. 3(b1) 3(b2), 3(c1), and 3(c2) originates from an effective “inverse Faraday effect” [32]. The transmission of a spin-polarized polaron through the HEF is in analogy to the case in which a local spin is irradiated by a proper circularly polarized light [33–37], where spin switching may take place depending on the light helicity. According to the principle of the inverse Faraday effect, an effective magnetic field, i.e., $\mathbf{M}_z \propto \mathbf{E}_h^* \times \mathbf{E}_h$, is generated along the z direction during the polaron transmission. The orientation of \mathbf{M}_z depends on whether the helix of the molecule is left- or right-handed, as seen from the propagating polaron. This effective magnetic field breaks the time-reversal symmetry and further leads to spin polarization. Figures 3(a1) and 3(a2) show that the time-reversal symmetry is maintained for a static polaron in the finite HEF; on the other hand, Figs. 2(b) and 2(c) show that spin selectivity does not take place for the polaron propagating through a conventional molecule with zero HEF either. Actually, to achieve clear spin selectivity, the following two conditions have to be satisfied simultaneously: (i) an effective SOC formed by a finite HEF and (ii) a charge (polaron) propagating through the HEF (realized by applying E_z). Such important ingredients were elsewhere alternatively elaborated as a “cumulative effect” [19]. That is, when an electron is passing through the chiral molecule, it visits each atom and orbits the nucleus. The helix structure ensures the orientations of the orbits visited by the electron bias toward a specific direction. Then the cumulative effect of the small magnetic field of the atomic SOC leads to a strong one which gives rise to the spin polarization. Obviously, the “visiting” of the electron and the finite SOC are both indispensable to achieve CISS. Our model agrees with and expands such a scenario to the polaron transport scheme.

The principle difference between our model and other theories is that the charge carriers are polarons rather than free charges. As a quasiparticle, the polaron (explicitly speaking, large polaron) exhibits a large size over 20 sites, which is determined primarily by the e - l coupling strength. It is natural to query the effect of the comparability between the polaron size and the helix pitch on the CISS. Figure 4(a) displays the evolution of SP at $eE_z\Delta z = 0.001t_0$ with varying N_0 . As shown, when $N_0 = 10$, i.e., one polaron ranges over two helix pitches, $SP = 0$. This is because the polaron cannot feel the varying of the HEF during its transport when its size is too large. The effective inverse Faraday effect is absent, and then both the spin-up and spin-down polarons pass through the chiral molecule without spin fluctuations. Increasing N_0 to 20, i.e., the polaron size is comparable to the helix pitch, CISS takes place, and SP reaches about 50%. Obviously, a relatively larger N_0 will be a benefit for the polaron to more clearly feel the HEF during transport. Further increasing N_0 will nonlinearly increase SP until it reaches saturation of about 70% at $N_0 = 40$.

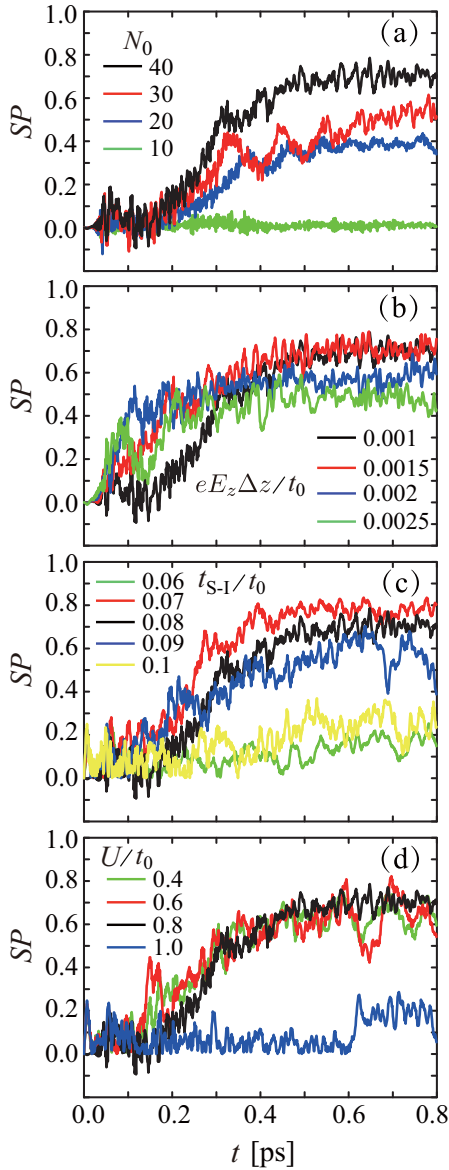


FIG. 4. Time evolutions of SP for different (a) N_0 , (b) E_z , (c) t_{S-1} , and (d) U .

As shown in Figs. 3(a1) and 3(a2), if the polaron is stationary, CISS does not occur, and $SP = 0$. However, if the drift velocity is too high, it is not a benefit to achieve a high SP either. Figure 4(b) displays the evolution of SP by fixing $N_0 = 40$ by tuning E_z (stronger E_z accelerate the polaron faster). It is shown that in the low-field regime, such as $eE_z\Delta z = 0.001t_0$, $0.0015t_0$, the SP can reach 70%. Further increasing E_z leads to a decrease of SP. The underlying physics is as follows. Two important timescales should be compared during polaron transport: one is the spin dephasing time under a HEF, and the other is the time interval of a polaron passing through one helix turn. If the latter timescale is much shorter than the former, the polaron spin cannot be effectively modulated by the HEF. In addition, we observe another two important trends with increasing E_z [38]: (i) polaron spins prefer to oscillate under higher E_z rather than switching to the steady opposite-orientation ones; (ii) the polaron localization is weakened, and

the polaron coherence is easily lost as time goes by. Then the transport carriers change to free charges; that is, the polaron-transport channel collapses. These two factors further lead to the decrease of SP.

Figure 4(c) further demonstrates time evolutions of SP for different t_{S-1} , keeping other parameters unchanged. As shown, in the regime of small t_{S-1} ($t_{S-1} \leq 0.06t_0$), SP is almost zero (green line). With increasing t_{S-1} , SP increases. At $t_{S-1} = 0.07t_0$, SP reaches its maximum value, which is greater than 70% (red lines). With further increasing t_{S-1} , however, the SP starts to reduce (see black, blue, and yellow lines). By checking the polaron's spin-lattice evolutions, we find that at $t_{S-1} = 0.1t_0$, the dynamics exhibits a behavior similar to that at a strong E_z ; namely, the polaron spins oscillate, rather than reverse. In addition, the polaron undergoes a delocalization, losing its coherence during propagation. Therefore, high SP is feasible only in the regime of the low external field and moderate SOC strength.

Electron-electron ($e-e$) correlation also affects the SP. It was theoretically reported that $e-e$ correlation would enhance SP of the current through a short chiral chain [39]. Figure 4(d) illustrates the dependence of SP on the on-site $e-e$ interaction. We find that, in the relatively weak U regime ($U = 0.4t_0$, $0.6t_0$, and $0.8t_0$), the SP is almost insensitive to U . However, when U is large, e.g., $U = 1.0t_0$, the SP is sharply decreased. At first glance, this result seems to contradict that reported in Ref. [39]. Actually, the difference in the effect of U on SP between our results and that presented in Ref. [39] stems from distinct dynamical processes. In our model, as the spin carrier is a polaron, the $e-e$ interactions' effect on SP is mainly ascribed to the polaron spin's response. If U is not too large, the spin density localized by polaron is mainly due to lattice distortions induced by the $e-l$ couplings; therefore, tuning U does not cause a significant change in SP. However, when U is large, the energy difference between the spin-up and spin-down states is enlarged. Then, a very strong effective magnetic field is required to reverse the spin. In contrast, such a polaron-spin reversal mechanism was not considered in Ref. [39], and the main transport mechanism was tunneling of free charges instead of polaron propagation. Hence, such a scenario was absent there.

IV. SUMMARY

We note that one comparative work was done recently [40] in which the lattice vibrations were treated as phonons. It was found that the lattice vibrations could induce additional conductance tunnelings and enhance the electronic coherence effect, which would increase SP. Undoubtedly, the degree of freedom of lattice vibrations is being regarded more and more as an important ingredient for achieving high SP.

In this work, we proposed a polaron transport mechanism in the chiral molecule to explain the CISS effect and high SP. We demonstrated that the different spin-orientated polarons exhibit distinct dynamics while passing through the HEF of a chiral molecule: the polaron whose spin orientation is parallel to its drift velocity direction keeps the spin state unchanged, while the others switch their spin to opposite orientations. The current generated by polaron transmission is thus spin orientation unified. Due to the strong coupling between spins

and lattices, the spin coherence is significantly enhanced, and thus, a very high SP greater than 70% can be achieved even with a relatively weak effective SOC. Different from the previously proposed scattering model, the spin-flip process in our model not only significantly enhances SP but also intensifies current intensity. To achieve a clear CISS effect, we suggest the helix pitch should be much larger than the polaron size. Furthermore, the external electric field applied to drive polarons should not be too large, and the SOC strength should not be too strong, so that the polaron does not lose coherence, leading to a decrease in SP. We hope our work will inspire more and more theoretical and experimental interest.

ACKNOWLEDGMENTS

This work was supported by the National Natural Science Foundation of China (Grants No. 11904254, No. 11974212, No. 11774203), the NSFC-Joint Foundation program of Shanxi Coal Based Low Carbon Nurturing Project (Grants No. U1710115, No. U1810204), the Platform and Base Special Project of Shanxi (Grant No. 201805D131012-3), and the Natural Science Foundation for Young Scientists of Shanxi Province (Grant No. 201901D211113). F.Q. is grateful for the financial support from CNPq and FAPDF-Finance Code 001, Brazil.

-
- [1] K. Ray, S. P. Ananthavel, D. H. Waldeck, and R. Naaman, *Science* **283**, 814 (1999).
- [2] R. Naaman and D. Waldeck, *J. Phys. Chem. Lett.* **3**, 2178 (2012).
- [3] R. Naaman, Y. Paltiel, and D. H. Waldeck, *Nat. Rev. Chem.* **3**, 250 (2019).
- [4] J. M. Abendroth, D. M. Stemer, B. P. Bloom, R. Roy, R. Naaman, D. H. Waldeck, P. S. Weiss, and P. C. Mondal, *ACS Nano* **13**, 4928 (2019).
- [5] R. Naaman and D. H. Waldeck, *Annu. Rev. Phys. Chem.* **66**, 263 (2015).
- [6] K. Michaeli, V. Varade V. R. Naaman, and D. H. Waldeck, *J. Phys.: Condens. Matter* **29**, 103002 (2017).
- [7] B. Göhler, V. Hamelbeck, T. Z. Markus, M. Kettner, G. F. Hanne, Z. Vager, R. Naaman, and H. Zacharias, *Science* **331**, 894 (2011).
- [8] Z. Xie, T. Z. Markus, S. R. Cohen, Z. Vager, R. Gutierrez, and R. Naaman, *Nano Lett.* **11**, 4652 (2011).
- [9] D. Mishra, T. Z. Markus, R. Naaman, M. Kettner, B. Göhler, H. Zacharias, N. Friedman, M. Sheves, and C. Fontanesi, *Proc. Natl. Acad. Sci. USA* **110**, 14872 (2013).
- [10] M. Kettner, H. Zacharias, D. Mishra, V. Kiran, R. Naaman, C. Fontanesi, D. H. Waldeck, S. Sek, J. Pawlowski, and J. Juhaniewicz, *J. Phys. Chem. C* **119**, 14542 (2015).
- [11] S. S. Skourtis, D. N. Beratan, R. Naaman, A. Nitzan, and D. H. Waldeck, *Phys. Rev. Lett.* **101**, 238103 (2008).
- [12] E. Medina, L. A. González-Arraga, D. Finkelstein-Shapiro, B. Berche, and V. Mujica, *J. Chem. Phys.* **142**, 194308 (2015).
- [13] S. Yeganeh, M. A. Ratner, E. Medina, and V. Mujica, *J. Chem. Phys.* **131**, 014707 (2009).
- [14] A. A. Eremko and V. M. Loktev, *Phys. Rev. B* **88**, 165409 (2013).
- [15] A. M. Guo and Q. F. Sun, *Phys. Rev. Lett.* **108**, 218102 (2012).
- [16] A. Dianat, R. Gutierrez, H. Alpern, V. Mujica, A. Ziv, S. Yochelis, O. Millo, Y. Paltiel, and G. Cuniberti, *Nano. Lett.* **20**, 7077 (2020).
- [17] V. V. Maslyuk, R. Gutierrez, A. Dianat, V. Mujica, and G. Cuniberti, *J. Phys. Chem. Lett.* **9**, 5453 (2018).
- [18] R. Gutierrez, E. Díaz, R. Naaman, and G. Cuniberti, *Phys. Rev. B* **85**, 081404(R) (2012).
- [19] S. Dalum and P. Hedegard, *Nano Lett.* **19**, 5253 (2019).
- [20] K. Nasu, *J. Phys. Soc. Jpn.* **53**, 302 (1984).
- [21] L. Zhang and S. Yamamoto, *J. Phys. Soc. Jpn.* **83**, 064708 (2014).
- [22] See Supplemental Material at <http://link.aps.org/supplemental/10.1103/PhysRevB.102.214303> for further details about the derivations of Eq. (4).
- [23] P. B. Woiczikowski, T. Kubar, R. Gutiérrez, R. A. Caetano, G. Cuniberti, and M. Elstner, *J. Chem. Phys.* **130**, 215104 (2009).
- [24] R. Gutiérrez, R. A. Caetano, B. P. Woiczikowski, T. Kubar, M. Elstner, and G. Cuniberti, *Phys. Rev. Lett.* **102**, 208102 (2009).
- [25] X. X. Li, X. F. Dong, J. Lei, S. J. Xie, and A. Saxena, *Appl. Phys. Lett.* **100**, 142408 (2012).
- [26] L. L. Zhang, S. J. Xie, and D. W. Kang, *Phys. Rev. E* **96**, 022414 (2017).
- [27] Y. Li, X. J. Liu, J. Y. Fu, D. S. Liu, S. J. Xie, and L. M. Mei, *Phys. Rev. B* **74**, 184303 (2006).
- [28] X. Liu, K. Gao, J. Fu, Y. Li, J. Wei, and S. Xie, *Phys. Rev. B* **74**, 172301 (2006).
- [29] S. Matityahu, Y. Utsumi, A. Aharony, O. Entin-Wohlman, and C. A. Balseiro, *Phys. Rev. B* **93**, 075407 (2016).
- [30] R. Naaman, Y. Paltiel, and D. H. Waldeck, *J. Phys. Chem. Lett.* **11**, 3660 (2020).
- [31] K. Michaeli and R. Naaman, *J. Phys. Chem. C* **123**, 17043 (2019).
- [32] G. H. Wagnière and G. L. J. A. Rikken, *Chem. Phys. Lett.* **502**, 126 (2011).
- [33] K. Vahaplar, A. M. Kalashnikova, A. V. Kimel, D. Hinzke, U. Nowak, R. Chantrell, A. Tsukamoto, A. Itoh, A. Kirilyuk, and Th. Rasing, *Phys. Rev. Lett.* **103**, 117201 (2009).
- [34] G. P. Zhang, T. Latta, Z. Babyak, Y. H. Bai, and T. F. George, *Mod. Phys. Lett. B* **30**, 16300052 (2016).
- [35] G. P. Zhang, Z. Babyak, Y. Xue, Y. H. Bai, and T. F. George, *Phys. Rev. B* **96**, 134407 (2017).
- [36] C. D. Stanciu, F. Hansteen, A. V. Kimel, A. Kirilyuk, A. Tsukamoto, A. Itoh, and Th. Rasing, *Phys. Rev. Lett.* **99**, 047601 (2007).
- [37] M. Berritta, R. Mondal, K. Carva, and P. M. Oppeneer, *Phys. Rev. Lett.* **117**, 137203 (2016).
- [38] See Supplemental Material at <http://link.aps.org/supplemental/10.1103/PhysRevB.102.214303> for further details about polaron spin dynamics under higher E_z .
- [39] J. Fransson, *J. Phys. Chem. Lett.* **10**, 7126 (2019).
- [40] G. F. Du, H. H. Fu, and R. Wu, *Phys. Rev. B* **102**, 035431 (2020).